EPJ manuscript No.
(will be inserted by the editor)

Family-Vicsek scaling of detachment fronts in Granular Rayleigh-Taylor instabilities during sedimentating granular/fluid flows

Jan Ludvig Vinningland[1,2], Renaud Toussaint[3,a], Michael Niebling[1,3], Eirik G. Flekkøy[1], and Knut Jørgen Måløy[1]

[1] Department of Physics, University of Oslo, P.O. Box 1048, 0316 Oslo, Norway
[2] International Research Institute of Stavanger, IRIS, P.O. Box 8046, 4068 Stavanger, Norway
[3] IPGS, University of Strasbourg, CNRS, 5 rue Descartes, 67000 Strasbourg

Abstract. When submillimetric particles are confined in a fluid such that a compact cluster of particles lie above the clear fluid, particles will detach from the lower boundary of the cluster and form an unstable separation front giving rise to growing fingers of falling particles. We study this problem using both experiments and hybrid granular/fluid mechanics models. In the case of particles from 50 to 500 microns in diameter falling in air, we study the horizontal density fluctuations at early times: the amplitude of the density difference between two points at a certain horizontal distance grows as a power law of time. This happens up to a saturation corresponding to a power law of the distance. The way in which the correlation length builds up to this saturation also follows a power law of time. We show that these decompaction fronts in sedimentation problems follow a Family-Vicsek scaling, characterize the dynamic and Hurst exponent of the lateral density fluctuations, respectively $z \sim 1$ and $\zeta \sim 0.75$, and show how the prefactors depend on the grain diameter. We also show from similar simulations with a more viscous and incompressible fluid, that this feature is independent of the fluid compressibility or viscosity, ranging from air to water/glycerol mixtures.

1 Introduction

In many natural and industrial situations, mixtures of granular materials and fluids are deformed. Physicists have intensively studied granular mechanics using discrete methods over the last 30 years [1,2] since the rise of powerful computers, to investigate various types of avalanche dynamics [3], the dynamics of sheared layers [4,5] and the stress distribution in sandpiles [6], to mention but a few. For sufficiently small grains, when the fluid seeps through the granular assembly, the resulting drag is sufficient to rearrange the grains, and it is necessary to take into account the momentum exchange between the granular and the fluid phase to understand the dynamics.

[a] e-mail: renaud.toussaint@unistra.fr

Such hybrid granular-fluid flows are manifested in many natural flows at the surface of the earth: e.g. in liquefaction [7], mudflows [8–10], or sand volcanoes. They also play a role in underwater avalanches and turbidites, or in sedimentation processes when large amounts of sediments are released and deposited. Eventually, their understanding are crucial for the mechanical stability in borehole exploration operations, during pumping in to or out of man-made wells, in hydrofracture [11], or for the understanding of reservoir stability and fault lubrication [12].

Elementary situations of sedimenting grains in a fluid and their stability have been recently studied in generic situations where a dense granular packing saturated with a fluid is subjected to a flow of the same fluid, as in the propagation of rising bubbles in air-grain flows in tubes, or the intermittency of flows in ticking hourglasses [13–15]. Experiments with dense granular packings displaced by pressurized air have been followed optically in Hele-Shaw cells [16–20], and studied numerically using models where the momentum exchange is based on a Darcy description of the flow with a grid resolution of a few grain diameters [21,22].

For example, when a granular packing in a circular cell where gravity acts perpendicularly to the cell walls starts to flow due to a sufficient air-overpressure in the centre, an instability corresponding to a granular Saffman-Taylor analog was observed [16,23]. Such analog behavior was also observed in linear cells, either with a free boundary at the outlet leading to decompaction [17,18], or with a confined flow for the particles leading to compaction [24,25]. Changing the properties of the interstitial fluid with orders of magnitudes in viscosity and compressibility (between oil and air) was shown to affect the dynamics of this process, but to lead to the formation of similar patterns [18].

When gravity is acting along the flow, a granular analog of the Rayleigh-Taylor instability has been studied: situations where initially a pack of dense grains are released into a zone of lighter fluid. The same fluid is also present in the interstitial space between the packed grains. This situation would naturally arise during sedimentation flows, e.g. when a sudden amount of compact material is released in open water. This instability has been studied with mixtures of grains (typically 100 µm in diameter) and air [19,26,27], and with less compressible and more viscous fluids such as water glycerol or oil [20,28,29].

The release of such dense packs of grains in a clear fluid contained in a closed cell, leads to the formation of a detachment front at the bottom of the pack. The particles fall faster from the bottom part than from the upper part of the pack, and fingers form in the previously clear fluid region. This front is unstable, grows fast in amplitude, and leads to coarsening bubbles empty of grains rising through the grain pack. The dynamics of this front has been studied using Fourier analysis by investigating the growth of each mode [19,26,30,31]. In this system, the change of the particle size, for sizes ranging from roughly 50 to 500 μm in diameter, was shown to leave the system dynamics invariant, using the grain diameter as the characteristic length scale.

We will show in this manuscript that the horizontal density profiles, as function of time and space, for different particle sizes, can be entirely collapsed and shown to follow a Family-Vicsek scaling. Such scaling, introduced by Family and Vicsek [32], was found to be obeyed by many surface growth processes. It relates the anomalous diffusion of a quantity, the growth of correlations, and the self affine geometry of the developed interface - or of the quantity characterized by this scaling [33]. For example, such a collapse was observed for the thermal fluctuations of magnetic hole assemblies, which are dipolar chains in thin fluid cells [34–36]. It is also obeyed by natural patterns slowly growing in rocks, as pressure solution seams evolve into stylolites [37–40].

This implies that a correlation length grows in this system, as a power law of time, $\xi \sim t^{1/z}$, with a dynamic exponent around $z \sim 1$. For scales above ξ, the root mean square of the lateral density fluctuations grows in a super-diffusive way, as $\sigma \sim t^{\beta}$

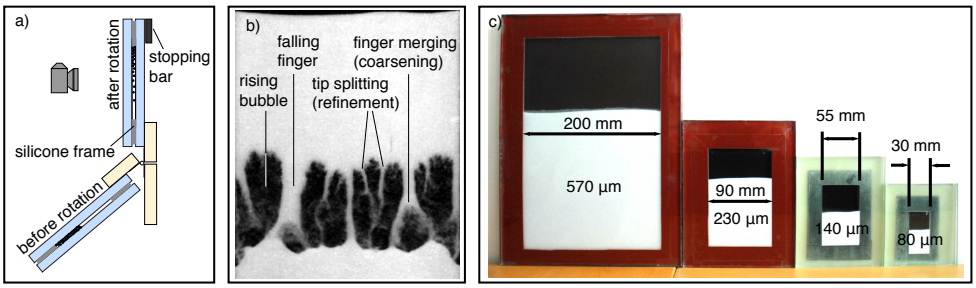

Fig. 1. (a) Experimental setup and principle, (b) typical granular Rayleigh-Taylor flow, where fingers of falling grains (white) form in the previously air-filled region (black) during an experiment, and (c) the experimental cells of different sizes with grains of proportional diameters.

with a growth exponent around $\beta \sim 0.75$. Below the correlation length, the density profiles are shown to be self-affine, with a Hurst exponent around $\zeta \sim 0.75$.

The Family-Vicsek scaling satisfied by the density fluctuations with these growth, Hurst and dynamic exponents is found to be universal for the granular Rayleigh-Taylor instability, in the sense that it is satisfied independently of the nature of the fluid over a rather large range of viscosities and compressibilities: we show here simulations performed both in lowly viscous and highly compressible air-granular mixtures, and in viscous and incompressible water/granular mixtures. They will be shown to follow the same Family-Vicsek scaling, with the same exponents: they belong to the same universality class. Note, however, that other surface growth processes follow Family-Vicsek scalings, but with different exponents (see [41] for many examples), and other growth processes do not display any such scaling. In particular cases, similar power laws are found between the fluctuation of the root mean square width as function of time and space, and the correlation length as function of time, but without the scaling relation between growth, Hurst and dynamic exponents $\beta = H/z$ obeyed in a Family-Vicsek scaling form. In this case, one has a reduced form of scaling called anomalous scaling [42].

In the next section, we will summarize the methodologies used to study the granular Rayleigh-Taylor instability, from an experimental and from a numerical perspective. Next, we will describe the types of patterns obtained at different particle sizes. Eventually, we will perform the Fourier analysis of the density fluctuations, and show that they can be collapsed at different times, for different wave numbers and for all investigated particle sizes on a master curve, displaying the fact that they follow a Family-Vicsek scaling.

2 Rayleigh-Taylor instability: definition and methods

2.1 Experimental setup

Historically, the Rayleigh-Taylor instability arises from a flat interface when a dense fluid is initially situated above a lighter one: in a closed container, the two fluids interchange positions while forming a fingering pattern. This instability, and the selection of a preferred wavelength due to the interplay between gravitational, capillary and viscous forces was first studied by Lord Rayleigh and I. G. Taylor [43,44]. The granular analog of this instability has been studied recently with air or more viscous fluids: it arises when initially a pack of dense grains is released on top of clear fluid

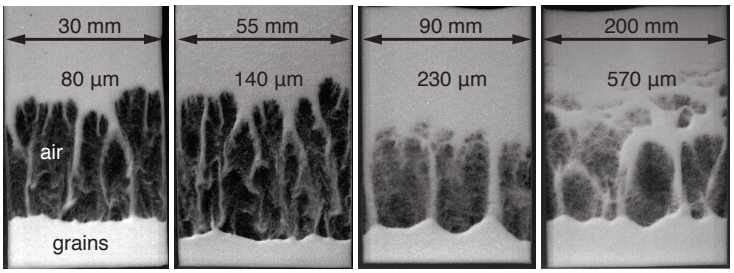

Fig. 2. Experimental snapshots of the granular Rayleigh-Taylor instability in air where the four cells shown in Fig. 1(c) are used.

in a closed vessel. There is no surface tension in this problem since the fluid is also initially present in the porous space between the grains in the upper pack.

The experiments are performed in a closed impermeable Hele-Shaw cell, which is initially prepared by letting grains accumulate at the bottom. The cell is then suddenly rotated to be brought upside down, and a damping bar stops the cell in a vertical direction, attenuating vibrations as much as possible. The setup is illustrated in Fig. 1(a). Several system sizes have been used for the air-grain experiments, ranging from 80 μm diameter to 570 μm diameter beads. The system sizes are proportional to the bead diameters, with system widths spanning from 30 to 200 mm, see Fig. 1(c). The grains used in the experiments where polystyrene spheres (Ugelstad spheres from Microbeads), with a density of 1.05 g/cm^3.

Early stages of the experimental pictures are shown on Figs. 1(b) and Fig. 2.

2.2 Simulation technique

The simulation techniques are described in details in [19] for the flow of grains and compressible air, or [20] for the flow of grains and incompressible viscous fluid.

In summary, the principle is as follows: the grains interact via repelling contact forces and via a drag force due to the flow of the interstitial fluid. This can be expressed as Newton's second law for each grain, as

$$ma = F_I + (\rho_g - \rho_f)g - \nabla P/\rho \tag{1}$$

where m and a are the grain mass and acceleration; F_I corresponds to the solid interaction forces with neighboring grains; the third term corresponds to buoyancy forces; the last term is seepage forces; g is gravity; ρ_f and ρ_g are the fluid and solid bulk mass densities; ρ is the number density of the grains: $\rho = V_g/(1-\Phi)$ with V_g the grain volume; Φ is the porosity. $P = P_T - \rho_f g z$ is the fluid pressure deviating from the hydrostatic profile – where P_T is the total fluid pressure and z the depth. This pressure is evaluated over a grid discretized at the representative elementary volume scale (the Darcy scale, a few grains large).

This equation is being solved at each time step, using a Verlet algorithm in molecular dynamic codes. The forces F_I are determined from elastic contact model [16,20], or from a contact dynamics scheme [19].

The dynamic equation solved for the fluid results from the following principles: mass conservation for the grains, mass conservation for the fluid, equation of state for the fluid, and Darcy's law to get the relative velocity between the fluid and the solid. Calling $\mathbf{u}$ the grain velocity, $\mathbf{v}$ the fluid velocity, and ρ_f the fluid density, this

can be expressed at the Darcy scale as

$$\partial_t(1-\Phi) + \nabla\cdot((1-\Phi)\,\mathbf{u}) = 0 \tag{2}$$

$$\partial_t(\rho_f\Phi) + \nabla\cdot(\Phi\rho_f\mathbf{v}) = 0 \tag{3}$$

$$\mathbf{v}-\mathbf{u} = -\frac{\kappa\nabla P}{\mu\Phi} \tag{4}$$

where μ is the fluid viscosity, κ is the local permeability of the packing, evaluated from the Carman-Kozeny equation

$$\kappa = \frac{d^2}{180}\frac{\Phi^3}{(1-\Phi)^2}$$

and the fluid mass conservation is expressed as one of the two alternatives: in general, linearizing this equation of state, one gets

$$\rho_f(P) = \rho_0\big(1+\beta\,(P-P_0)\,\big)$$

where β is the fluid compressibility, P_0 an initial (reference) pressure, and ρ_0 the fluid density at that pressure.

This set of equations leads to the following reduced form:

$$\Phi\,(\partial_t P + \mathbf{u}\cdot\nabla P) = \nabla\cdot\left(\hat{P}\frac{\kappa}{\mu}\nabla P\right) - \hat{P}\nabla\cdot\mathbf{u} \tag{5}$$

where $\hat{P} = \rho_f/(\rho_0\beta) = P - P_0 + 1/\beta$

Considering air as a perfect gas, this reduces to $\rho_f = \rho_0 P/P_0$, $\beta = 1/P_0$ and $\hat{P} = P$, so that

$$\Phi\,(\partial_t P + u\cdot\nabla P) = \nabla\cdot\left(P\frac{\kappa}{\mu}\nabla P\right) - P\nabla\cdot u \tag{6}$$

which is solved alternately with the molecular dynamic time steps, using a Cranck-Nicholson algorithm [45].

For a viscous fluid considered as incompressible, we have $\beta = 0$, $\rho_f = \rho_0$. and the equation 5 in the limit $\hat{P}\to\infty$, reduces to

$$\nabla\cdot\left(\frac{\kappa}{\mu}\nabla P\right) = \nabla\cdot u$$

which is solved at each time step using a multigrid algorithm [45].

2.3 Dynamics of the granular Rayleigh-Taylor instability

In both experiments and simulations, for grains falling in air or in water/glycerol, the dynamics can be qualitatively described as follows: From the initial configuration where grains are packed above the clear fluid region, the dense grains start to flow downward, i.e. sediment, while the fluid passes through the grains. This situation leads to the formation of fingers of particles detaching from the lower boundary of the upper compact pack. These fingers of particles regroup, and bubbles of low particle density form in the pack, rise and coalesce. This dynamics is illustrated in Fig. 2 (experimentally) and Fig. 3 (numerically), for the air-grain case, and in Fig. 4 for the incompressible fluid-grain case.

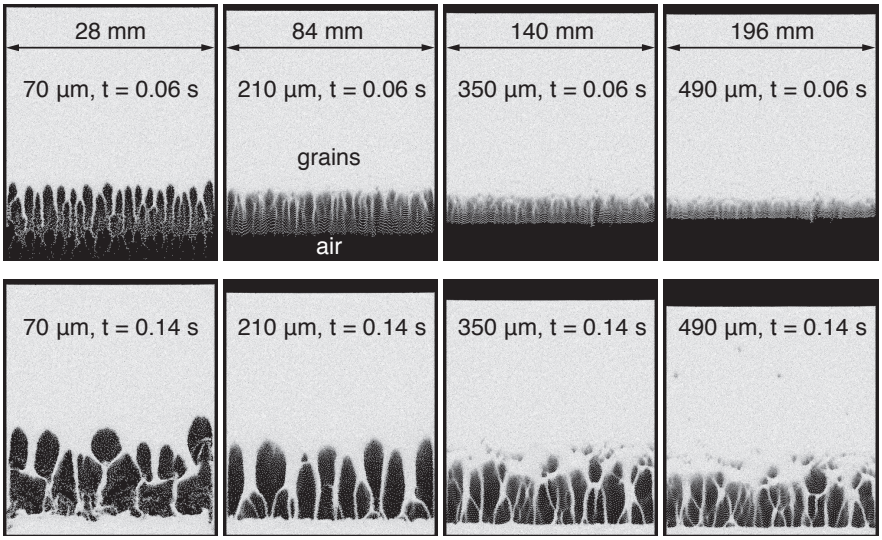

Fig. 3. Simulation at four different grain/system sizes (horizontal axis) at two different times (vertical axis) showing the development of the instability with the initial front destabilization in the top row.

We notice that at low viscosities, simulations with incompressible fluids are reminiscent of the dynamics obtained with compressible air. As the viscosity is increased (from top to bottom in Fig. 4), the fingers get mixed more rapidly as they detach from the lower front of the compact pack. The grains have here a size of 140 microns in diameter, and a density of 2.5 g/cm^3, the fluid has the density of water.

One way to analyze the instability of the detachment front, at the bottom of the compact pack, is to compute horizontal density profiles. In this way, it is possible to measure the lateral growth of density fluctuations, while the fingers form and regroup. This can be done at each horizontal level at vertical coordinate y and time t, extracting density fronts as function of the horizontal variable x, $\rho(x, y, t)$. This is illustrated in Fig. 5.

The most variable profiles as function of x are just below the detachment front: the particle density is roughly constant (at a scale above a few grains) in the compact packing above the detachment front, and constant and low in the empty region below. Hence, to increase the statistical quality of the quantity we analyze, we perform the average over all horizontal profiles at a given time, and obtain in this way horizontal density profiles $\rho(x, t) = \langle \rho(x, y, t) \rangle_y$. For the experiments, the density is not known directly, but the same procedure is performed on the basis of light intensity (pixel gray value) recorded with a fast camera.

These horizontal density functions are then spatially Fourier transformed, and their Fourier power-spectra are represented at various times and for various grain sizes using a bi-logarithmic scale, as is shown in Fig. 6 for the simulations, and in Fig. 7 for the experiments. The inset plots represent the raw power spectra for all sizes, and the full figures indicate the power spectra using the grain diameters as a unit size. The comparison between inset and main plot shows the size collapse.

The experiments and simulations with compressible air have been analyzed as function of the particle size. Snapshots of the early times of these simulations with variable particle sizes are shown in Fig. 2. A spatial rescaling using the grain diameter rendered the pattern formation mechanism similar for the range of diameters investi-

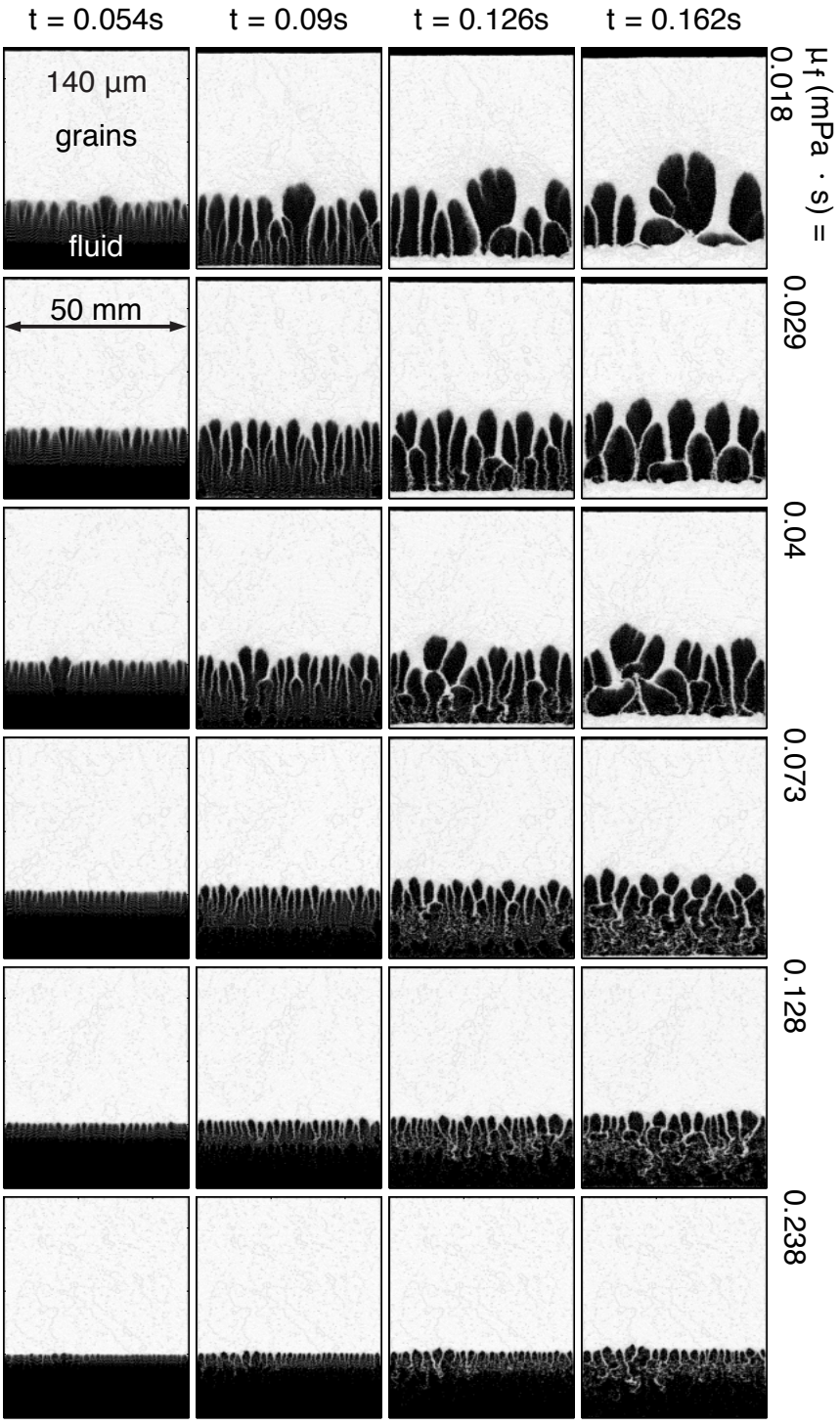

Fig. 4. Numerical simulations of grains sedimenting in an incompressible fluid of variable viscosities μ_f (increasing from top to bottom). Time runs from left to right.

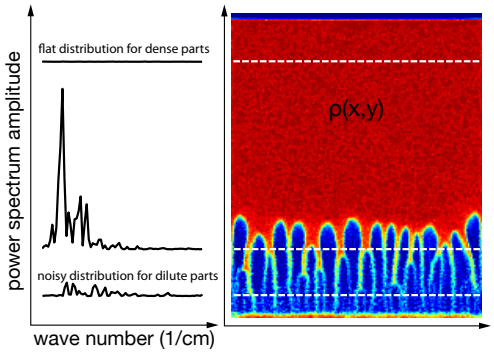

Fig. 5. Extraction of a density function under the dense plug (middle dashed line in the right figure), and computation of its Fourier power spectrum (left).

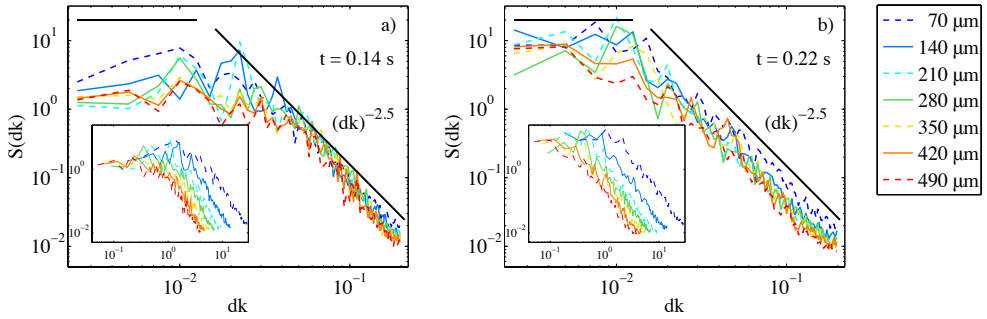

Fig. 6. Power spectrum collapse at two different times for air-grain simulations with grains of different diameters d. The inset plot shows the unscaled power spectra, $S(k)$, whereas a spatial scaling by the grain diameter yields collapsing $S(dk)$ in the main plot.

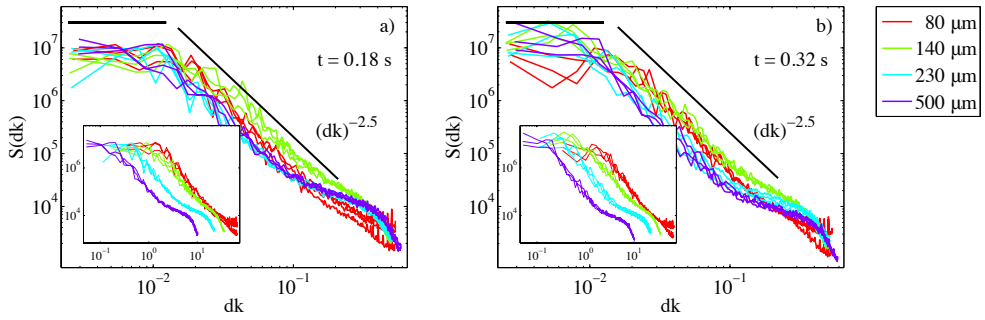

Fig. 7. Power spectrum collapse at two different times for air-grain experiments with grains of different diameters d. The inset plot shows the unscaled power spectra, $S(k)$, whereas a spatial scaling by the grain diameter yields collapsing $S(dk)$ in the main plot, apart from deviations at the smallest scales.

gated. This was studied in details in [27]. The rescaling is illustrated by the collapse of the structures analyzed in Fig. 6 (for simulations) and Fig. 7 (for experiments), obtained after rescaling the spatial units with the grain diameter, d. The insets in these figures show the density profiles prior to rescaling.

3 Family-Vicsek scaling of the lower decompaction front

In the plots of the Fourier transformed density profiles in Figs. 6 and 7, one notes that, both for the experiments and for the simulations, the low wavenumber part of the spectra is flat. This corresponds to spatially uncorrelated density fluctuations for large scales (with a white noise character), whereas the power spectrum decreases as a power-law for small scales (high wavenumber). A behavior

$$S(k,t) \sim k^{-2.5}$$

is observed on this part, both for experiments and for simulations. The cutoff k_c corresponds to the maximum size of the density fluctuations, $\xi = 2\pi/k_c$, called the correlation length. The power-law behavior for scales smaller than the correlation length corresponds to the self-affine character of these density fluctuations. The power spectrum distribution of a self-affine quantity may be expressed as

$$S(k,t) \sim k^{-(1+2\zeta)},$$

which in our case yields a Hurst exponent $\zeta \sim 0.75$.

Deviations are observed for the experiments in Fig. 7 on the smallest scales, which can be attributed to a different dynamics at scales of the order of the plate separation.

Interestingly, when the case of incompressible fluids is compared, a similar behavior is observed as for the compressible case, see Fig. 8. This behavior extends to the whole range of viscosities probed, from 0.018 to 0.9 mPa·s, almost three orders of magnitude. This is the case despite the obvious difference between the developed stages of the instability, as is seen by comparing Figs. 3 and 4. The early stages, however, seem to follow the same type of behavior with respect to the lateral spreading of the density fluctuations.

The Family-Vicsek scaling behavior is summarized in the plots in Fig. 9 for the compressible case, and in Fig. 10 for the incompressible case. For the compressible case, the transformed density functions $S(k,t,d)$ for all the probed grain sizes d and for times $t \leq 0.23$ s all fall on a single master curve shown in Fig. 9(a). For the incompressible case there is, however, a deviation from the Family-Vicsek scaling for the early times and largest viscosities probed, as seen in the incomplete collapse for the first times in Fig. 10(c).

The observed Family-Vicsek scaling merely reflects the following about the power spectrum $S(k,t)$:

$$S(k,t) = Ck^{-1-2\zeta} g(dk(t/\tau)^{1/z}) \tag{7}$$

$$g(x) \sim C_1 x^{1+2\zeta} \quad \text{for } x \ll 1, \text{ i.e. } 1/k \gg \xi \text{ with } \xi \sim t^{1/z} \tag{8}$$

$$g(x) = C_2 \qquad \text{for } x \gg 1, \text{ i.e. } 1/k \ll \xi\,, \tag{9}$$

where τ is a time-constant and C,C_1 and C_2 are constants. So that $S(k,t)$ is independent of k for scales above the correlation length ξ, and independent of t when the mode k has saturated, with a wavelength $1/k$ exceeding the correlation length. This leads to a generalized diffusion behavior

$$S(k,t) \sim t^{(1+2\zeta)/z} \tag{10}$$

when $1/k > \xi$, and

$$S(k,t) \sim k^{-(1+2\zeta)} \tag{11}$$

when $1/k < \xi$.

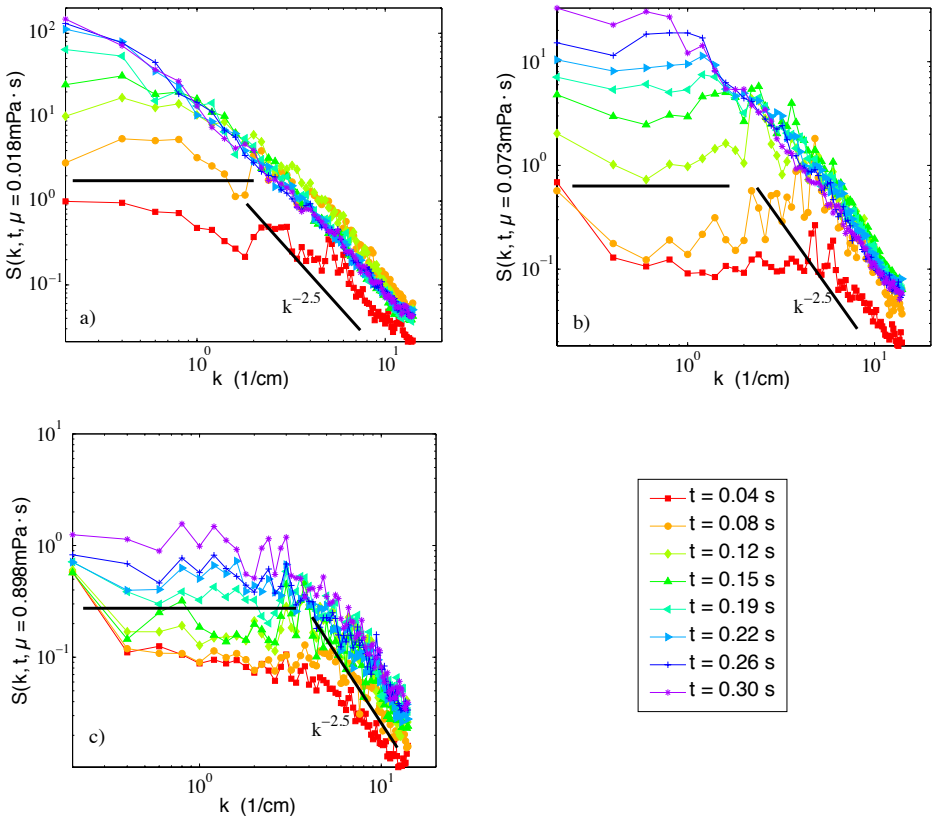

Fig. 8. Power spectra of the horizontal density profile for different times: results of simulations in an incompressible fluid. The viscosities of the fluids are respectively (a): 0.018, (b): 0.073 and (c): 0.9 mPa·s. The different curves correspond to different times after the start of the instability.

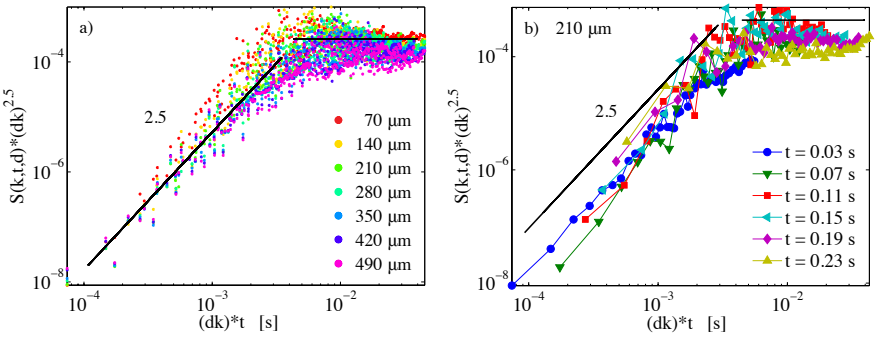

Fig. 9. Family-Vicsek scaling obtained from numerical data. (a) shows the scaling for all grain sizes and for $t \leq 0.23$ s, while (b) is the same plot as (a) but only showing the 210 μm data and where the colors indicate the time from blue (early times) to yellow (late times).

This corresponds, in real space, to a behavior for the root mean square of the solid density

$$\sigma_\rho = \langle \rho^2 - \langle \rho \rangle^2 \rangle^{1/2}$$

following a Family-Vicsek scaling that can be obtained form Parseval's theorem, as

$$\sigma^2(L,t) = (1/L) \int_{k=2\pi/L}^{\infty} S(k,t) dk \tag{12}$$

$$= (1/L) \int_{k=2\pi/L}^{\infty} C k^{-1-2\zeta} g(dk(t/\tau)^{1/z}) dk \tag{13}$$

$$= (t/\tau)^{(2\zeta)/z} (1/L) \int_{2\pi(t/\tau)^{1/z}/L}^{\infty} k' g(k') dk' \,, \tag{14}$$

i.e.

$$\sigma(L,t) = (t/\tau)^\beta F(L/t^{1/z})$$

with

$$\beta = \zeta/z \,,$$

where L is the width of the system. Hence, the density profile under the detachment front saturates as a self-affine function [33] with a Hurst exponent $\zeta \simeq 0.75$ for scales below ξ, and displays a super-diffusive behavior with an exponent $\beta \simeq 0.75$. The root mean square of the solid density, $\sigma_\rho = \langle \rho^2 - \langle \rho \rangle^2 \rangle^{1/2}$ displays a behavior corresponding to

$$\sigma_\rho \sim t^\beta .$$

Conversely, for scales l above ξ, one has a self-affine behavior,

$$\langle (\rho(x+l) - \rho(x) \rangle^2 \sim l^{2\zeta} \,.$$

The correlation length ξ is increasing as a power law with time, as $\xi \sim t^{1/z}$. The density in the detachment front exhibits these behaviors with respectively dynamic, Hurst and growth exponents

$$z = 1 \tag{15}$$

$$\zeta = 0.75 \tag{16}$$

$$\beta = \zeta/z = 0.75 \tag{17}$$

One can also equivalently express the Family-Vicsek scaling with a scaling function g, such as:

$$S(k,t) = C(dk)^{-2.5} g(dk(t/\tau)) \tag{18}$$

$$g(x) \sim C_1 x^{2.5} \quad \text{for } x \ll 1, \text{ i.e. } 1/k \gg \xi \text{ with } \xi \sim t \tag{19}$$

$$g(x) = C_2 \qquad \text{for } x \gg 1, \text{ i.e. } 1/k \ll \xi \,. \tag{20}$$

Indeed, $S(k,t) * (d*k)^{2.5} = C g(d*k*t/\tau)$ is represented for air-grain simulations in Fig. 9, and this scaling function master curve displays these two expected behaviors for the granular-gas flow.

This is also the case for the granular-incompressible fluid flows, as shown in Fig. 10 for three viscosities. As observed in the previous representation, the collapse is rather followed, apart from the earliest times at larger viscosities.

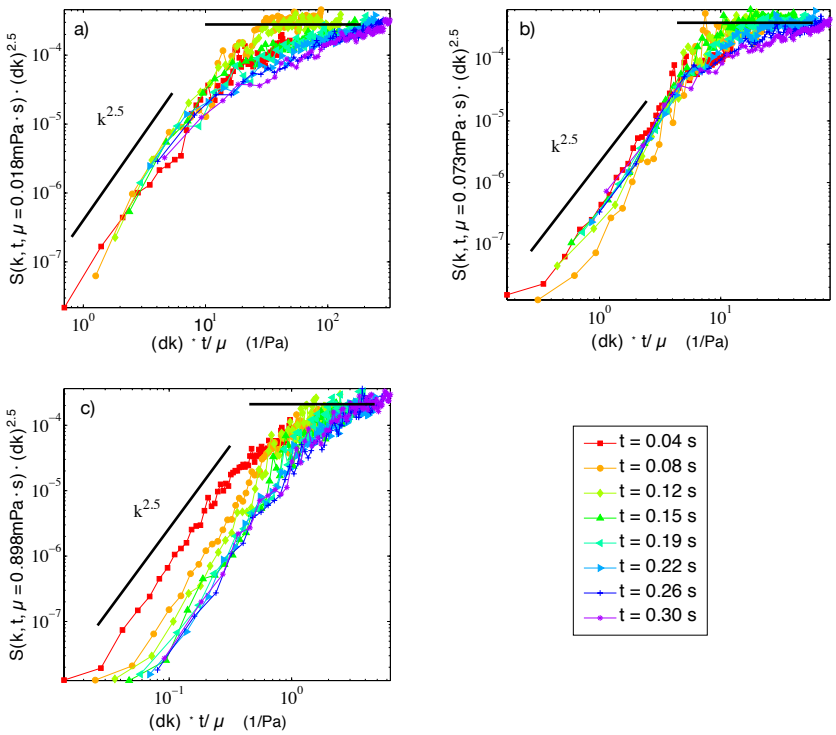

Fig. 10. Master function intervening in the Family-Vicsek scaling for the Rayleigh-Taylor instability in incompressible fluids: Scaled power spectra $S(k,t)*(d*k)^{2.5}$, which are functions g of $d*k*t/\tau$, with a behavior $g(x) \sim C_1 x^{2.5}$ at small arguments, and $g(x) \sim C_2$ at large ones. The Hurst exponent used for the scaling is 0.75, and the dynamic exponent is 1. The viscosities of the fluids are respectively (a): 0.018, (b): 0.073 and (c): 0.9 mPa·s.

4 Conclusion

We have studied situations where well packed cohesionless grain assemblies, heavier than the fluid between them, are released in a clear fluid. This gives rise to the so-called granular Rayleigh-Taylor instability, where bubbles empty of grains rise, while granular fingers form in the clear fluid region.

The principles of hybrid simulations starting from basic physical equations was established, for both cases where the carrier fluid is a perfect gas or an incompressible viscous fluid. The experimental setup and results are also shown to be consistent with the simulations in the air-grain case.

Grains are mixed during this process, and one can follow the evolution of spatial correlations in lateral density fluctuations, with vertically averaged horizontal grain density profiles $\rho(x)$. These density fluctuations are shown to follow an anomalous diffusion behavior with a growth exponent $\beta \sim 0.75$. Hence, for two points at a large horizontal distance x from each other, a difference in density will grow as $\delta\rho(x,t) \sim t^{\beta}$. The density fluctuations will follow this behavior up to a saturation when the correlation length ξ reaches x. ξ is growing as a power-law of time, with a dynamic exponent around 1. Eventually, for scales larger than ξ, the density profile displays a self-affine behavior, with a Hurst exponent around 0.75. This is seen in the spatial

Fourier domain, both for experiments and simulations for air-grain systems, and for simulations for mixtures of grains and incompressible viscous fluid.

Eventually, we have shown that the power-spectra of the density at all times can be collapsed according to a Family-Vicsek scaling.

References

1. Herrmann, H.J., J.-P. Hovi and S. Luding, editors, *Physics of dry granular media*, (NATO ASI Series E: Applied Sciences, vol. 350, Kluwer Academic Publishers, Dordrecht/Boston/London 1998)
2. Duran, J., *Sands, powders and grains*, (Springer, New York 2000)
3. Altshuler, E., R. Toussaint, E. Martinez, O. Sotolongo-Costa, K.J. Måløy and J. Schmittbuhl; "Revolving rivers in sandpiles: from continuous to intermittent flows", Phys Rev E, **77** (2008) 031305. doi:org/10.1103/PhysRevE.77.031305
4. Aharonov, E. and D. Sparks, Shear profiles and localization in simulations of granular material, Phys. Rev. E **65**, (2002) 051302.
5. Aharonov, E. and D. Sparks, Stick-slip in granular material, J. Geophys. Res. **109**, (2004) B09306, DOI:10.1029/2003JB002597.
6. Reydellet G. and E. Clement, Response functions in granular pilings, Phys.Rev.Lett. **86**, (2001) 3308.
7. Goren, L., E. Aharonov, D. Sparks and R. Toussaint, Pore pressure evolution in deforming granular material: A general formulation and the infinitely stiff approximation, J. Geophys. Res., **115**, (2010) B09216. doi:10.1029/2009JB007191
8. Travelletti, J., C. Delacourt, P. Allemand, J.-P. Malet, J. Schmittbuhl, R. Toussaint and M. Bastard, Correlation of multi-temporal ground-based images for landslide monitoring: application, potential and limitations, submitted to ISRPS Journal of Photogrammetry and Remote Sensing, (2011) revised.
9. Malet, J.-P., D. Laigle, A. Rematre and O. Maquaire. Triggering conditions and mobility of debris flows associated to complex earthflows. Geomorphology **66** (2005) 215-235.
10. van Asch, Th.W.J. and J.-P. Malet, . Flow-type failures in fine grained soils: an important aspect in lanslide hazard analysis. Natural Hazards and Earth System Sciences **9**, (2009) 1897-1909.
11. E. G. Flekkøy, A. Malthe-Sørenssen, and B. Jamtveit. Modeling hydrofracture. J. Geophys. Res., **107 (B8)** (2002) 2151.
12. Goren, L., E. Aharonov, D. Sparks and R. Toussaint, The mechanical coupling of fluid-filled granular material under shear, P.A.Geoph. **168**, (2011) 12, in press. doi: 10.1007/s00024-011-0320-4
13. Le Pennec T., K.J. Maloy, E.G. Flekkoy, J.C. Messager and M. Ammi, Silo hiccups: Dynamic effects of dilatancy in granular flow, Phys. of Fluids **10**, (2008) 3072-3079. doi:10.1063/1.869835
14. E. G. Flekkøy, S. McNamara, K. J. Måløy, and D. Gendron. Structure formation and instability in a tube of sand. Phys. Rev. Lett. **87**, (2001) 134302.
15. D. Gendron, H. Troadec, K. J. Måløy, and E. G. Flekkøy. Bubble propagation in a pipe filled with sand. Phys. Rev. E, **64** (2001) 021509.
16. Johnsen, Ø., R. Toussaint, K.J. Måløy and E.G. Flekkøy, Pattern formation during central air injection into granular materials confined in a circular Hele-Shaw cell, Phys. Rev. E **74**, (2006) 011301. doi:10.1103/PhysRevE.74.011301
17. Johnsen, Ø., R. Toussaint, K.J. Måløy, E.G. Flekkøy and J. Schmittbuhl, "Coupled air/granular flow in a linear Hele-Shaw cell", Phys Rev E **77**, (2007) 011301. doi:10.1103/PhysRevE.77.011301
18. Johnsen, Ø., C. Chevalier, A. Lindner, R. Toussaint, E. Clément, K.J. Måløy, E.G. Flekkøy and J. Schmittbuhl, Decompaction and fluidization of a saturated and confined granular medium by injection of a viscous liquid or a gas, Phys. Rev. E **78** (2008) 051302. doi:10.1103/PhysRevE.78.051302

19. Vinningland, J.L., Ø Johnsen, E.G. Flekkøy, R. Toussaint and K.J. Måløy, A granular Rayleigh-Taylor instability: experiments and simulations, Phys. Rev. Lett. **99**, (2007) 048001. doi:10.1103/PhysRevLett.99.048001
20. Niebling, M.J., E.G. Flekkøy, K.J. Måløy, R. Toussaint, Mixing of a granular layer falling through a fluid", Phys. Rev. E **82**, (2010) 011301. doi: 10.1103/PhysRevE.82.011301
21. S. McNamara, E. G. Flekkøy, and K. J. Måløy. Grains and gas flow: Molecular dynamics with hydrodynamic interactions. Phys. Rev. E **61**, (2000) 40544059.
22. D. V. Anghel, M. Strauß, S. McNamara, E. G. Flekkøy, and K. J. Måløy. Erratum: Grains and gas flow: Molecular dynamics with hydrodynamic interactions. Phys. Rev. E **74**, (2006) 029906(E).
23. Cheng, X., L. Xu, A. Patterson, H.M. Jaeger and S.R. Nagel, Towards the zero-surface-tension limit in granular fingering instability, Nat. Phys. **4**, (2008) 234–237. doi:10.1038/nphys834
24. Niebling, M.J., R. Toussaint, E.G. Flekkøy and K.J. Måløy, Dynamic aerofracture of dense granular packings, submitted to Phys. Rev. Lett. (2011).
25. Schelstraete, M., Suivi de la dcompaction et arofracturation de matriaux faiblement consolids, Master thesis, University of Strasbourg (2009).
26. Vinningland, J.L., Ø. Johnsen, E.G. Flekkoy, R. Toussaint and K.J. Måløy, Experiments and Simulations of a gravitational granular flow instability, Phys. Rev. E **76**, (2007) 051306. doi:10.1103/PhysRevE.76.051306
27. Vinningland, J.L., Ø. Johnsen, E.G. Flekkøy, R. Toussaint and K.J. Måløy, Influence of particle size in Rayleigh-Taylor granular flow instability, Phys. Rev. E **81**, (2010) 041308. doi: 10.1103/PhysRevE.81.041308
28. Niebling, M.J., E.G. Flekkøy, K.J. Måløy, R. Toussaint, Sedimentation instabilities: impact of the fluid compressibility and viscosity, Phys. Rev. E **82**, (2010) 051302. doi: 10.1103/PhysRevE.82.051302
29. C. Völtz, W. Pesch, and I. Rehberg. Rayleigh-taylor instability in a sedimenting suspension. Phys. Rev. E **65** (2001) 011404.
30. Vinningland, J.L., Ø. Johnsen, E.G. Flekkøy, R. Toussaint and K.J. Måløy, Granular Rayleigh-Taylor instability, in *Proc. of the 6th international conference on micromechanics of granular media, Powder and grains 2009*, M. Nakagawa and S. Luding, editors.
31. Vinningland, J.L., Ø. Johnsen, E.G. Flekkøy, R. Toussaint and K.J. Måløy, Granular Rayleigh-Taylor instability, *Proc. of the Traffic and Granular Flow conference, 2007, Orsay, 2009*.
32. F. Family and T. Vicsek, J. Phys. A **18** (1985) L75.
33. A.-L. Barabasi and H.E. Stanley, *Fractal Concepts in Surface Growth*, Cambridge University Press, Cambridge 1995).
34. Toussaint, R., G. Helgesen and E.G. Flekkøy, Dynamic roughening and fluctuations of dipolar chains, Phys. Rev. Lett., **93**, (2004) 108304. doi:10.1103/PhysRevLett.93.108304
35. Toussaint, R., J. Akselvoll, G. Helgesen, E.G. Flekkøy and A.T. Skjeltorp, Interactions of magnetic holes in ferrofluid layers, Progress in Colloid and Polymer Science, **128**, (2004) 151. doi:10.1007/b12355
36. Toussaint, R., E.G. Flekkøy, and G. Helgesen, The memory of fluctuating brownian dipolar chains, Phys. Rev. E **74**, (2006) 051405. doi:10.1103/PhysRevE.74.051405
37. Schmittbuhl, J., F. Renard, J.P. Gratier and R. Toussaint, Roughness of stylolites: Implications of 3D high resolution topography measurements , Phys. Rev. Lett. **93**, (2004) 238501.
38. Koehn, D., F. Renard, R. Toussaint, C. Passchier The development of stylolite teeth and their relation to stress and finite compaction, EPSL, **257**, (2007) 582. doi:10.1016/j.epsl.2007.03.015
39. Rolland, A., R. Toussaint, P. Baud, J. Schmittbuhl, N. Conil, D. Koehn, F. Renard and J. P. Gratier, Modeling stylolites in sedimentary rocks, submitted to JGR B. (2011).
40. Laronne Ben-Itzhak, L., E. Aharonov, A. Sagy and R. Toussaint, Upper bound on stylolite roughness as indicator for the duration and amount of dissolution, submitted to EPSL (2011).

41. Fereydoon Family and Tamàs Vicsek, eds, *Dynamics of Fractal Surfaces* (World Scientific, Singapore New Jersey London Hong Kong 1991)
42. López, Juan M., Scaling Approach to Calculate Critical Exponents in Anomalous Surface Roughening, Phys. Rev. Lett., **83**, 1999, 4594.
43. Rayleigh, Lord. Investigation of the character of the equilibrium of an incompressible heavy fluid with variable density. Proc. London Math. Soc. **14** (1883) 170-7.
44. Drazin, P.G. and W.H. Reid, *Hydrodynamic stability, 2nd ed.* (Cambridge University Press, Cambridge 2004).
45. Press et al., *Numerical Recipes*, Cambridge University Press, 1992